

Structured Materials: Magnetic Structures and Electronic Properties

Z. Q. Qui,
Chairman

Electron beam stimulated spin reorientation

T. L. Monchesky,^{a)} J. Unguris, and R. J. Celotta

Electron Physics Group, National Institute of Standards and Technology, Gaithersburg, Maryland 20899

(Presented on 15 November 2002)

Using scanning electron microscopy with polarization analysis, we observed the electron beam induced switching of the magnetic state of epitaxial single-crystal Fe(110) films grown on atomically flat cleaved GaAs(110). For low film thickness the magnetization lies along the $[-110]$ in-plane direction, while above a thickness of 19 monolayers, the ground state magnetization configuration switches to the $[001]$ in-plane direction. If Fe films are grown to a thickness greater than the critical thickness of the reorientation, the magnetization is caught in a metastable state, oriented along $[-110]$. We discovered that we can locally switch the metastable state to the stable $[001]$ direction by irradiating the metastable magnetic state with a suitable electron current density. The reversal proceeds by the nucleation and growth of lancet-shaped domains that move in discrete jumps between pinning sites. Our results show that there is a permanent reduction of the strength of defect sites without a permanent change in the overall anisotropy. We demonstrate how an electron beam can be used to locally control domain structure. [DOI: 10.1063/1.1556250]

We have discovered that epitaxial ultrathin Fe films can be prepared in a metastable magnetic state that can be locally switched by the electron beam from a scanning electron microscope (SEM). The surface anisotropy of Fe/GaAs(110) has an easy axis along the in-plane $[-110]$ direction, perpendicular to the $[001]$ bulk easy-axis direction. Below a critical thickness, t_{crit} , the stable direction of the magnetization points along $[-110]$. Above t_{crit} , $[001]$ becomes the stable direction.¹ However, when we grow a film through t_{crit} , we find the magnetization is frozen in a $[-110]$ metastable state. Subsequently, we discovered that we can switch the magnetization into the stable $[001]$ configuration by irradiating the sample with an electron beam of appropriate strength.

The GaAs(110) surface was prepared by cleaving either 0.5- or 1.0-mm-thick wafers *in situ*. Scanning tunneling microscope measurements show that surfaces prepared in this fashion are atomically flat over areas several microns wide.² The two-dimensional reflection high-energy electron diffraction (RHEED) pattern composed of sharp spots demonstrated the high surface quality of the cleaved GaAs surface. An electron beam evaporator deposited Fe wedges on room temperature GaAs(110) with a shutter that varied the exposure of the Fe flux along the length of the substrate. All wedges in this study had their thickness gradient along $[-110]$. The film thickness was calibrated by spatially resolved RHEED intensity oscillations.³ Scanning electron microscopy with polarization analysis (SEMPA)⁴ was used to image the magnetic structure of our films at remanence. SEMPA simultaneously measures two in-plane components of the magneti-

zation and the topography of the sample surface. Beam currents ranged between 1 nA and 10 nA and the beam voltage was fixed at 10 keV.

When we grew Fe wedges on GaAs(110) we expected to see a reorientation transition from $[-110]$ to $[001]$ near a thickness of 24 monolayers (ML), assuming the surface magnetocrystalline anisotropy of Au/Fe(110) is not substantially different than that of a vacuum/Fe(110).⁵ SEMPA measurements made directly following growth showed this not to be the case. The magnetic moments of nearly the entire sample pointed along the $[-110]$ direction. The dashed curve in Fig. 1 shows that the $[-110]$ direction is the energy minimum of the anisotropy energy for the thinnest films. The magnetization is trapped in a metastable state when the thickness is increased above t_{crit} since the global minimum for low thicknesses changes to a local minimum, as illustrated by the solid curve in Fig. 1

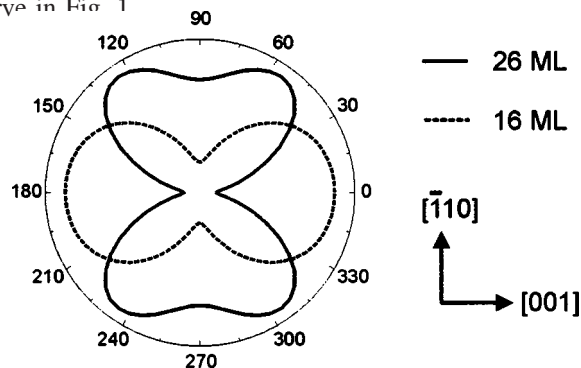


FIG. 1. The magnetocrystalline anisotropy energy of Au/Fe/GaAs(110) as a function of angle with respect to the $[100]$ crystallographic direction, calculated from the anisotropy measurements of Ref. 5. The solid line is the energy of a 26 ML Fe film ($t > t_{\text{crit}}$) and the dashed line is that of a 16 ML Fe film ($t < t_{\text{crit}}$). The plots are scaled for comparison.

^{a)}Electronic mail: theodore.monchesky@dal.ca

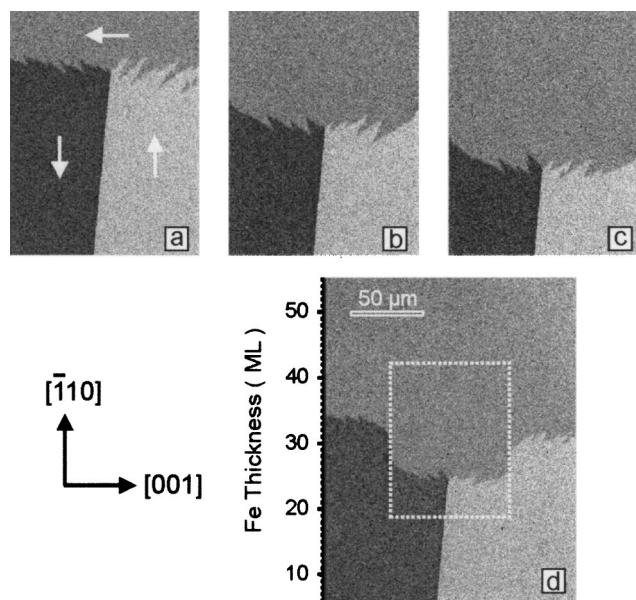


FIG. 2. (a)–(c) A sequence of $83\ \mu\text{m} \times 63\ \mu\text{m}$ SEMPA images of a domain wall moving down an Fe wedge on GaAs(110). The electron beam does not uniformly illuminate the region of interest: a 1 nA electron beam is rastered with discrete steps of $0.3\ \mu\text{m}$ with a spot size of roughly $0.02\ \mu\text{m}$. The region above the wall is stable and the region below the wall and above a thickness of roughly 20 ML is metastable. The electron beam is rastered from top to bottom and then right to left. The frames were collected continuously, each requiring 10.5 min. The time between the frames shown here is 84 min. The arrows in (a) indicate the direction of the magnetization. (d) A $175\ \mu\text{m} \times 133\ \mu\text{m}$ SEMPA image of the region investigated in (a)–(c), indicated by the dashed rectangle.

We also observed a few regions with $[100]$ orientation. These regions are typically found next to macroscopic defects. We hypothesize that the defects nucleate $[100]$ oriented domains either by changing the anisotropy over a large enough region or by the magnetostatic field nucleating closure domains. These stable domains are typically seen at higher thickness, where the anisotropy energy barriers are lower.

The electron microscope beam was then used to enlarge these stable domains at the expense of the metastable domains. The electron beam stimulates the reorientation; the domain wall moves to a position along the edges of the region the electron beam has scanned. As the domain wall approaches the thinner end of the wedge, at some point, which varies from sample-to-sample, it stops moving into the electron beam scanned region. If true equilibrium were achieved, t_{trans} (the minimum wedge thickness at the domain wall position) would equal t_{crit} . A $t_{\text{trans}} = 19\ \text{ML}$ was the lowest value observed in this system. Figures 2(a), 2(b), and 2(c) shows the motion of a stable $[100]$ domain under the influence of the electron beam. The final distortion of the once straight magnetic domain wall, shown in the larger area scan of Fig. 2(d), was achieved by scanning over an $83\ \mu\text{m} \times 63\ \mu\text{m}$ region for 3 h with a 1 nA current.

The domains in motion in Fig. 2 exhibit lancet-shaped supplementary domains because of magnetostatics. A wall at a 45° angle to both the $[-110]$ and $[100]$ directions is preferred because it keeps the normal component of the magnetization continuous across the wall. In place of one wall

along $[100]$, two different wall orientations combined to create a lancet: one wall is at an angle of roughly 15° from the 45° or zero magnetic charge orientation, and the other wall is at an angle of roughly -15° . Unlike the out-of-plane spin-reorientation transition,⁶ there is no collapse of the magnetic domain size at t_{trans} .

The wall velocity depends on film thickness. In Figs. 2(a), 2(b), and 2(c) the wall velocity decreased from 4 to 2 nm/s while moving down the wedge from a film thickness of 36 ML to 26.5 ML, while under the influence of a 1 nA beam. A velocity of 6.4 nm/s was observed at 55 ML. The reduction in wall velocity with film thickness correlates with the increase in the anisotropy energy barrier that separates the metastable and stable configurations. This suggests that the strength of the pinning sites is related to the effective anisotropy that is determined by the bulk anisotropy plus the surface anisotropy weighted by the film thickness. The motion is not smooth, i.e., the wall makes jumps between pinning sites at a speed much faster than can be imaged with SEMPA. The velocities reported here are the average distances the wall travels per unit time as it moves down the wedge.

The wall velocities at a given thickness were very sensitive to the quality of the substrate and varied by up to a factor of 20 from sample-to-sample. For a good cleave with mirror like surfaces there are virtually no defects visible to the electron microscope. In this case, the wall velocities are over 100 nm/s for a 40 ML thick film and a 1 nA beam. This is in contrast to the sample of Fig. 2 that has a substrate surface with step bunches visible to the SEM and a wall velocity in the 40 ML region of 4.6 nm/s. This large sample-to-sample variation in wall velocity suggests that the dominant pinning sites are related to the Fe–GaAs interface. The switching is also sensitive to the electron beam parameters, although a given set of electron beam parameters produces different results depending on the substrate condition. In general, increasing the current or current density will increase the wall velocity. We have also observed wall motion that continues at a slower rate independent of observation by the electron beam; in Fig. 2 this drift is 0.8 nm/s for a 36 ML thickness.

To determine whether adsorbates play a role in the electron beam switching, we covered the Fe wedge with 0.6 nm of Au. When Fe is grown on GaAs, As is known to segregate to the Fe surface.⁷ Furthermore, we find carbon and oxygen on the surface of Fe after long exposure to the residual gases in the vacuum chamber. The addition of the Au layer dropped the wall velocity by an order of magnitude suggesting that the Au altered domain wall pinning sites at the Fe surface. Since the Au cap does not prevent the electron beam from being able to move the domain wall, adsorbate diffusion or desorption can be ruled out as a switching mechanism.

The effect of an external field was investigated by first applying a field along the $[100]$ direction of a 0 ML to ML wedge. The thickness of the wedge increased by 1 ML every $6.51 \pm 0.02\ \mu\text{m}$ along $[-110]$. A 110 kA/m (1.4 kOe) field pushed the t_{trans} to 33 ML. A small raster scan, indicated by the white box in Fig. 3(b), further reduced t_{trans} to 28.5 ML

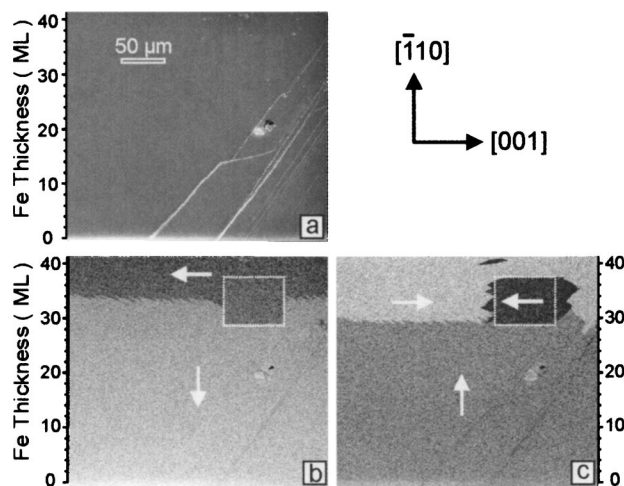


FIG. 3. The influence of a magnetic field on an Fe wedge/GaAs(110). (a) $304\ \mu\text{m} \times 271\ \mu\text{m}$ secondary electron intensity of the wedge. (b) The corresponding SEMPA image after the sample was placed in a 110 kA/m (1.4 kOe) field along [100]. The $71\ \mu\text{m} \times 54\ \mu\text{m}$ region previously irradiated by the electron beam with $5.92 \times 10^{-6}\ \text{C}$ is indicated by the white dashed line. (c) The SEMPA image of the same region in (b) after the sample was placed in a magnetic field of 110 kA/m, applied along $[-110]$.

over a $71\ \mu\text{m}$ length region. This shows that a 110 kA/m field is not sufficient to bring the sample into equilibrium and indicates that the pinning fields of the 33 ML region are very roughly of that strength.

We then investigated the reversibility of the electron beam induced switching by attempting to switch a stable state back into a metastable one. A 110 kA/m magnetic field⁸ was applied along the $[-110]$ direction but it did not push the t_{trans} to higher film thickness. Surprisingly, the field reduced the metastable domain by moving t_{trans} to 28.5 ML over the entire length of the sample, as illustrated in Fig. 3(c). Also, evidence of the previous $71\ \mu\text{m} \times 54\ \mu\text{m}$ scan is present in the form of a reverse domain, shown in Fig. 3(c), further demonstrating that the electron beam permanently altered the sample in this region.

The wedge was then capped with 0.6 nm Au in order to compare the t_{trans} to a previously published critical thickness. A magnetic field applied along [100] was used to help the system approach equilibrium. SEMPA images show that $t_{\text{trans}} = 25.4 \pm 0.3\ \text{ML}$. The wall that separates the two domains zigzags about this average with a peak-to-peak amplitude of 1.4 ML. This transition agrees well with $t_{\text{crit}} = 24 \pm 1.2\ \text{ML}$ for Au/Fe/GaAs(110) as determined by magneto-optic Kerr effect measurements.⁵ Furthermore, a 10 nA current could not change t_{trans} , an additional indication that $t_{\text{trans}} = t_{\text{crit}}$. This demonstrates that the electron beam does not permanently affect the average anisotropy of the sample, but instead modifies the anisotropy of a relatively small number of pinning sites. This finding is in contrast to electron stimulated switching of the magnetization of Co films on Pt(111),⁹ where it was suggested that a 10 nA beam was able to modify the average anisotropy of the Co by as much as 30%.

There are two switching mechanisms that can be immediately ruled out. The first is the magnetic field from the electron beam. For a 1 nA beam, the maximum magnetic

field is roughly $0.2\ \mu\text{T}$. This is several orders of magnitude smaller than the coercive field even for the best quality Fe crystals. The second mechanism that can be ruled out is electron beam heating of the crystal lattice, also ruled out in Ref. 9. Based on calculations presented in Ref. 10, the maximum possible increase in temperature of the surface of the crystal is of the order of 0.1 K for a 1 nA, 10 keV beam.

We speculate that there may be two processes involved in the electron beam induced switching of the sample: one process permanently reduces the pinning strength, and the other process temporarily weakens the remaining anisotropy energy barrier. One possible origin of the temporary change in anisotropy is excitations in the Fe film created by the electron beam. Magnetocrystalline anisotropy is known to be very sensitive to the Fermi level filling.¹¹ It has been recently shown that the electron excitations from a femtosecond laser pulses can alter the anisotropy sufficiently to create a spin-reorientation transition.¹² In a similar fashion, the electronic excitation from an electron beam will populate states above the Fermi level that can alter the anisotropy. This possibility is consistent with our recent measurements of bcc Co grown on GaAs(110).¹³ We have found an in-plane spin-reorientation transition in contrast to previous reports.¹⁴ When the Co thickness reaches 8 ML there is a reorientation from $[-110]$ to $[100]$ without an in-grown metastable state: no domain wall motion was observed. Based on calculations and spin-polarized photoemission, it has been shown that the band structure of bcc-Co is very similar to that of Fe with one additional electron.¹⁵ If the electronic excitations produced by the incident electron beam cause the Fe to temporarily behave similarly to Co, they will remove the metastable state and allow the Fe to reach equilibrium.

In conclusion we have demonstrated that metastable states can be created in Fe/GaAs(110) by growing epitaxial films to thicknesses greater than t_{crit} . These states can be switched with the help of an electron beam. The electron beam permanently reduces the strength of the pinning sites without permanently affecting the overall magnetocrystalline anisotropy that creates the metastable and stable configurations.

This work is supported in part by the Office of Naval Research. T.L.M. would like to acknowledge financial support from the Natural Sciences and Engineering Research Council of Canada.

¹G. A. Prinz, G. T. Rado, and J. J. Krebs, J. Appl. Phys. **53**, 2087 (1982).

²J. A. Strosio (private communication).

³J. Unguris, R. J. Celotta, and D. T. Pierce, J. Appl. Phys. **75**, 6437 (1994).

⁴D. T. Pierce, J. Unguris, and R. J. Celotta, *Ultrathin Magnetic Structures* (Springer, New York, 1994), pp. 117–147.

⁵R. Höllinger *et al.*, J. Appl. Phys. **89**, 7136 (2001).

⁶M. Speckmann *et al.*, Phys. Rev. Lett. **75**, 2035 (1995).

⁷T. L. Monchesky *et al.*, Phys. Rev. B **60**, 10242 (1999).

⁸This is an order of magnitude larger than the coercive field along $[-110]$.

⁹R. Allenspach *et al.*, Appl. Phys. Lett. **73**, 3598 (1998).

¹⁰L. Reimer, *Scanning Electron Microscopy: Physics of Image Formation and Microanalysis* (Springer, New York, 1998).

¹¹G. H. O. Daalderop *et al.*, Phys. Rev. B **50**, 9989 (1994).

¹²F. Kronast *et al.* (unpublished).

¹³T. L. Monchesky, J. Unguris, and R. J. Celotta (unpublished).

¹⁴G. A. Prinz, Phys. Rev. Lett. **54**, 1051 (1985).

¹⁵G. A. Prinz *et al.*, J. Appl. Phys. **57**, 3024 (1985).